Atmos. Chem. Phys. Discuss., 10, 24763–24780, 2010
www.atmos-chem-phys-discuss.net/10/24763/2010/
doi:10.5194/acpd-10-24763-2010

Atmospheric Chemistry and Physics Discussions

Optical properties of pristine ice crystals in mid-latitude cirrus clouds: a case study during CIRCLE-2 experiment

J.-F. Gayet[1], G. Mioche[1], V. Shcherbakov[1,2], C. Gourbeyre[1], R. Busen[3], and A. Minikin[3]

[1]Laboratoire de Météorologie Physique, UMR 6016 CNRS/Université Blaise Pascal, France
[2]LaMP – Institut Universitaire de Technologie de Montluçon, Avenue A. Briand-BP 2235, 03101 Montluçon Cedex, France
[3]Deutsches Zentrum für Luft- und Raumfahrt, Institut für Physik der Atmosphäre, Oberpfaffenhofen, Germany

Received: 22 September 2010 – Accepted: 8 October 2010 – Published: 22 October 2010

Correspondence to: J.-F. Gayet (j.f.gayet@opgc.univ-bpclermont.fr)

Published by Copernicus Publications on behalf of the European Geosciences Union.

Abstract

Preferential horizontally-oriented ice crystals with a prevalent hexagonal-plate shape revealed by the Cloud Particle Imager can explain systematic larger Lidar CALIOP extinctions when compared with extinction derived from co-located in situ measurements. Surprisingly, the Polar Nephelometer does not reveal any signature of 22° (and 46°) halos, showing a rather featureless scattering phase function in this case. In contrast, well pronounced 22° halo peaks are observed with predominant similar-shaped ice crystals in other cirrus situations. This paper discusses the results of a careful examination of CPI images with Polar Nephelometer observations in order to explain occurrence and non occurrence of the 22° halo feature. Observations highlight that halo peaks are evidenced only by the presence of perfect plate ice crystals (or pristine crystals). On the basis of previous data sets in mid-latitude cirrus it is found that simple pristine crystals are uncommon whereas particles with imperfect or complex shapes are prevalent. As a result, phase functions are smooth and featureless and best represent cirrus scattering properties.

1 Introduction

Light-scattering properties of ice crystals have been the subject of considerable work over the last few years, addressing the global climate effect of cirrus clouds (Stephens et al., 1990). Optical phenomena such as 22° halo (and 46° halo) were first explained by Mariotte (1717) as being due to refraction of light (in the visible) by randomly oriented hexagonal ice crystals. Modelling studies of scattering phase functions show that these features are an indication of highly regular pristine ice crystals (see among others Ping Yang et al., 2001). Observations of cloud ice particles tend to show much smoother scattering behaviour compared with modelling results obtained in laboratory studies (Sassen and Liou, 1979; Crépel et al., 1997; Barkey et al., 2002). The first in situ observations of azimuthal scattering patterns also confirmed that smooth scattering

ACPD
10, 24763–24780, 2010

phase functions prevail in cirrus clouds (Gayet et al., 1998; Auriol et al., 2001; Gayet et al., 2004). Defaults in crystal geometry, roughness of the ice surface or imperfect internal structure are known to hamper the formation of halos (see among others Baran and Labonnote, 2007). This may explain the rare ground-observed occurrences of these optical phenomena. In this paper we describe two cases of in situ observations of mid-latitude cirrus clouds, both having mostly planar-plate ice crystals but showing significant differences in optical properties in terms of 22° halo occurrences. Surprisingly, for one case, the Polar Nephelometer data do not reveal any signature of 22° (and 46°) halos although preferential horizontal orientation of the plate-shaped crystals does cause systematic larger retrieved Lidar CALIOP extinctions (due to specular scattering effects onto the crystal surfaces) compared with collocated in situ measurements (Mioche et al., 2010). For the second case, well-marked 22° halo features are observed in a few cloud portions along with prevalent planar-plate ice crystals. The interpretation of these results is discussed in the light of a careful analysis of the ice particle morphologies and by using a theoretical model of light scattering (Shcherbakov et al., 2006a). Implications for realistic modelling of scattering properties of cirrus clouds are given.

2 The CIRCLE-2 experiment and aircraft instrumentation

The CIRCLE-2 campaign, held from 4 to 26 May 2007, involved two Falcon (F20) aircraft. The first one, operated by DLR (Deutsches Zentrum für Luft- und Raumfahrt), was equipped with microphysical and optical in situ probes. The second Falcon, from SAFIRE (Service des Avions Français Instrumentés pour la Recherche en Environnement), was carrying remote sensing Radar-Lidar (RALI) downward-looking system operated by IPSL (Institut Pierre Simon Laplace) (Protat et al., 2004). The two aircraft were operated from Oberpfaffenhofen (near Munich, Germany) and from Creil (near Paris, France), respectively. In this paper, we will discuss cloud in situ observations made by the DLR Falcon.

ACPD
10, 24763–24780, 2010

Four independent techniques for cloud in situ measurements were installed onboard the Falcon: the PMS FSSP-300 operated by the DLR, the Cloud Particle Imager (CPI), the Polar Nephelometer (PN) and the PMS 2D-C probe, operated by the Laboratoire de Météorologie Physique (LaMP). The combination of these four techniques provides a description of particles within a diameter range varying from a few micrometers (typically 3 µm) to about 2 mm. The method of data processing, the reliability of the instruments and the uncertainties of the derived microphysical and optical parameters have been described in detail by Gayet et al. (2009). Relative humidity was derived from measurements using a CR-2 frost point hygrometer. The derivation method of the vertical airspeed from the Falcon aircraft measurements has been described in Bögel and Baumann (1991). An error of ±10 cm/s for a mean value within a flight path of 200 km (or about 20 min flight duration) is generally expected.

In the following section, we will discuss cirrus optical properties measured with the Polar Nephelometer for two well identified cases characterized, respectively by non-occurrence and occurrence of a 22° halo feature. These optical observations will be compared with the ice particle shapes recognized from the Cloud Particle Imager data.

3 Results

3.1 Cirrus properties with non-occurrence of 22° halo (case A)

A representative example of cirrus properties with non-observed 22° halo feature (case A) is illustrated from observations carried out during a flight co-ordinated with CALIPSO overpass on 16 May 2007 in a thin frontal cirrus located to the west of France over the ocean (Mioche et al., 2010). Figure 1 represents the time-series of the vertical component of the airspeed and cloud parameters: the concentration of ice particles with d >50 µm (from 2D-C data), the extinction coefficient, the asymmetry parameter and the halo ratio (these two last parameters being measured by the Polar Nephelometer). Since the Polar Nephelometer measures the scattered energy at scattering

ACPD
10, 24763–24780, 2010

angles of 22° and 18.5°, the ratio of these two energy values provides a quantitative criteria (called hereafter halo ratio) which characterizes the 22° halo feature (Auriol et al., 2001). High halo ratio (>1.0) reveals sharp peaks with well-pronounced 22° halo whereas smoothed peaks and/or smoothed scattering phase functions with no 22° halo are characterized by smaller halo ratio (<1). The sampling levels were located near the cirrus cloud top: 12000 m/−59°C (from 13:30 to 13:45) and 11 600 m/−55°C (from 13:47 to 13:57, see Fig. 1). The results show that the extinction coefficient is 0.3 km^{-1} on average whereas the ice particle concentration detected by the 2D-C reaches only 1 to 3 l^{-1}. The asymmetry parameter and the halo ratio exhibit very small horizontal variations indicating homogeneous optical properties. Mean properties (averaged between 13:32:15 and 13:47:20) are displayed in Fig. 2. The upper left panel shows the mean particle size distributions of the FSSP-300, 2D-C and CPI whereas the upper right panel represents the scattering phase function (without normalization in units of μm^{-1} sr^{-1}) measured by the Polar Nephelometer (filled black circle symbols) and the theoretical phase function (cross symbols) calculated from the FSSP-300 size distribution assuming (spherical) ice crystals. The mean values of the parameters indicate ice particle concentration (1.4 cm^{-3}), concentration of particle with d>100 µm (0.3 l^{-1}), ice water content (2 mg/m^3), extinction coefficient (0.28 km^{-1}), effective diameter (21 µm) and asymmetry parameter (0.788). The observed and the theoretical phase functions (see upper right panel) show close agreement at the forward scattering angles (5°–50°). Because most of the extinction is caused by scattering at forward angles, this proves the consistency of data from the FSSP-300 and Polar Nephelometer instruments. According to Heymsfield (2007), the FSSP-300 and Polar Nephelometer measurements are not likely to be strongly affected by ice crystal–shattering effects since the largest particles are less than 250 µm in size.

On Fig. 1, the time-series of the CPI particle shape classification for ice crystals larger than 25 µm has been superimposed (averaged over 5 s. due to low particle concentration and expressed in percentages for each categories). The LaMP software (Lefèvre, 2007) was used to process CPI images to provide information on the ice-

ACPD
10, 24763–24780, 2010

particle morphology. The results show that plate ice crystals dominate the ice crystal shape in the whole reported cloud sequence. We note in passing, that such plate ice crystals could be horizontally oriented (Bréon and Dubrulle, 2004) which may therefore explain, for that particular cirrus situation, the significant overestimation of the retrieved CALIPSO extinction with regards to coordinated in situ observations (Mioche et al., 2010). On the bottom left panel on Fig. 2, pie-chart representation of the average particle shape classification (in terms of particle surface) reveals 42% plates, 10% needles and columns with 48% unclassified particles (irregular) as illustrated by examples of ice particle images (see bottom right panel). Even with the prevalence of regular plate-shaped ice crystals, the Polar Nephelometer surprisingly does not reveal any signature of 22° halo with a featureless scattering phase function as highlighted on Fig. 2 with a halo ratio of 0.74. It should be noted that this feature is not a consequence of the preferential orientation of plate-like crystals because the orientation is lost inside the shrouded Polar Nephelometer (and CPI) inlet due to aerodynamical disturbances (King, 1986). Therefore randomly oriented plate-like crystals should have caused a sharp peak in the forward scattering properties related to the 22° halo (see among others Ping Yang et al., 2001) which is not observed in this case.

A counterexample is discussed in the next section which describes cirrus properties with a well marked 22° halo peak still related to plate-like ice crystals.

3.2 Cirrus properties with 22° Halo occurrence (case B)

This example (case B) concerns cirrus cloud sampled over France on 16 May 2007 during the DLR Falcon transit flight from Oberpfafenhoffen to Brest (France). The flight level was −27°C/7100 m. Time-series of the same parameters as in Fig. 1 with relative humidity (over ice) are displayed in Fig. 3. Compared with the previous example, the cirrus cloud is denser with rather high horizontal heterogeneities. The extinction coefficient and the ice particle concentration peak at 4.8 km^{-1} and 50 l^{-1}, respectively while the asymmetry parameter and halo ratio reveal large variations (from 0.77 to 0.80 and from 0.5 to 1.4, respectively). These variations, when compared to the CPI particle

ACPD
10, 24763–24780, 2010

shape classification for ice crystals, highlight that high halo ratio (22° halo peaks) are observed with the largest occurrence of plate ice crystals (see arrows on Fig. 3). In order to illustrate this feature the mean properties (averaged between 09:02:10 and 09:02:30, i.e. during 20 s, see Fig. 3) are displayed on Fig. 4. As for Fig. 2, the upper panels display the mean particle size distributions and measured scattering phase function along with the theoretical phase function calculated from the FSSP-300 size distribution. At forward angles (see upper right panel) the observed energy (PN) is larger than the theoretical phase function derived from FSSP-300 data indicating a significant contribution of particles larger than 20 µm on the scattering pattern. The mean values of the parameters indicate the ice particle concentration (1.9 cm^{-3}), the concentration of particles with d>100 µm (7.3 l^{-1}), the ice water content (14 mg/m^3), the extinction coefficient (0.49 km^{-1}), the effective diameter (86 µm) and the asymmetry parameter (0.795). Within this cloud sequence the Polar Nephelometer clearly reveals the 22° halo peak which remarkably occurs with mostly pristine plate-shaped ice crystals. Indeed, the pie-chart (see bottom left panel on Fig. 4) reveals 57% plates, 17% columns and needles, 12% of dendrite and side plane with only 15% unclassified (irregular). Compared to the previous classification on Fig. 2, the smaller proportion of unclassified shapes is explained by larger ice crystals (86 µm versus 21 µm, respectively) due to a more reliable shape recognition. The plate type is found to be the dominant ice crystal shape for both examples with rather similar occurrences (57% versus 42%, respectively).

As larger ice crystals are observed in this case (crystal sizes up to 1 mm), the FSSP-300 and Polar Nephelometer measurements are likely to be more greatly affected by ice crystal shattering effects than in the previous cirrus case. From a modelling approach (Shcherbakov et al., 2010), rough estimates of subsequent errors on extinction and particle concentration could be estimated as 35% and 70%, respectively. Nevertheless, a visual analysis of the CPI images (see examples on Fig. 4d) clearly suggests that most of the sampled ice crystals are intact with a quasi-perfect shape and a dense internal structure. Such a robust feature may be less sensitive to the particle shattering.

ACPD
10, 24763–24780, 2010

4 Discussion and conclusions

If the prevalence of plate ice crystals is a common feature of both the examples given above, larger ice crystals are observed for case B as exemplified on Fig. 5a which displays the halo ratio versus the mean volume diameter (MVD) derived from the CPI size distributions. Well-marked 22° halo peaks (halo ratio >1) are found for *MVD* ranging from 50 to 250 µm. Case A data (non halo case) represented by red symbols are distributed over a smaller *MVD* range (<130 µm) and with sizes larger than 20 µm. This size appears to delineate the lower limit of ice crystal size responsible (at visible wavelengths) for halo formation according to earlier laboratory studies (Sassen and Liou, 1979, Barkey et al., 2002) and theoretical results (Mishchenko and Macke, 1999). In situ observations at the South Pole station (Shcherbakov et al., 2006a, Lawson et al., 2006) also reported very well-marked 22° halo peaks with pristine ice crystals no larger than 100 µm. Therefore, the reported ice crystal sizes do not appear critical for the halo/no-halo interpretation.

A careful examination of the CPI images reveals that most of the recorded ice crystal plates on Fig. 4d present a relatively regular shape with a perfectly transparent internal structure. Indeed, refraction through the 60° prisms of such plates will produce a very sharp scattering peak near 22°. If quite regular plate-shaped ice particles are also highlighted from CPI images on Fig. 2d, the main difference in crystal morphology, compared with images on Fig. 4d, is the imperfect internal structure with including well recognizable lattices. This proves the consistency of our observations, namely that the halo feature is evidenced only by the presence of perfect plate ice crystals (or pristine crystals, strictly speaking). This also means that the Polar Nephelometer data contains a signature of pristine ice crystals. Defaults in crystal geometry, roughness of the ice surface or imperfect internal structure do hamper the formation of halo (see among others Baran and Labonnote, 2007). The model from Shcherbakov et al. (2006a) has been used to compute the angular scattering patterns by using measured crystal shape and size and by considering both roughness and internal structure. In this model,

ACPD
10, 24763–24780, 2010

the surface roughness assumes the Weibull statistics and the air bubble density is hypothesized to represent the internal heterogeneities of the crystal. Ice plates and columns were modelled by quasi-hexagonal prisms with the aspect ratio of 0.2 and 2, respectively. To smooth the 46° halo peak, the hexagonal planes were divided into a number of facets. Furthermore, the vertices of the facets were randomly shifted along the "C" axis of the crystal. The shift was within 10% of the crystal length. The particle shape classification was considered in terms of particle surface (see pie-charts on Figs. 2c and 4c). The fitting results are shown using red points on Figs. 2b and 4b. The smoothed scattering pattern (Fig. 2b) was obtained for the very rough surface of crystals with a heavy load of inclusions. The scattering pattern with 22° halo (Fig. 4.b) was computed for the slightly rough surface of crystals that have no inclusions.

The azimuthal halo pattern of the scattering behaviour significantly enhances the asymmetry parameter as exemplified on Fig. 5b. The larger g is (from 0.780 to 0.805) more pronounced in the 22° halo peak (0.74 < halo ratio <1.50), simply because the energy is scattered more in the forward direction. Highly regular or pristine ice crystals are expected to result from extremely regular crystal growth. Figure 5c and d display the scatter plots of the halo ratio versus relative humidity (over ice) and vertical air-speed, respectively. Figure 5c reveals that the 22° halo peaks are distributed mostly at around 100% of RHi and confirm the findings from Heymsfield (1986) and Pruppacher and Klett (1997) that low ice supersaturations are known to favour regular and slow crystal growth. This feature should be found in low updraft velocities but results on Fig. 5d rather show that halo ratios are more pronounced for increasing updrafts.

Coming back to Fig. 3, pristine ice crystals (CPI images) with subsequent 22° halo signature (PN) are observed in only a few cloud portions (see arrows) characterized by small horizontal scales (from 1000 m to 4000 m). The large data set obtained during the INCA experiment showed that cloud sections with occurrence of the halo signature (and therefore pristine ice crystals) occurred statistically in only 3% of the total measurement time in mid-latitude cirrus (Auriol et al., 2001; Gayet et al., 2004; Shcherbakov et al., 2006b). Korolev et al. (2000) also observed a similar low occurrence (3%) of

ACPD
10, 24763–24780, 2010

pristine ice particles in Arctic clouds (with temperatures lower than −30°C) from the analysis of CPI data. This means that while simple pristine crystals are uncommon, particles with imperfect or complex shapes (shape defaults, roughness, inclusions, . . .) are prevalent. Following the findings of Baran (2004) modelling of ice crystal ensemble rather than single crystals should better represent cirrus single-scattering properties. Our large data set in cirrus (at mid-latitudes) clearly shows that phase functions are smooth and featureless and best represent scattering properties from cirrus.

Acknowledgements. This work was funded by the Centre National d'Etudes Spatiales (CNES) and by a grant from the CNRS/INSU. The contribution of DLR as well as large part of Falcon flight hours was funded in the framework of the DLR PAZI-2 project. We thank the members of DLR (Deutsches Zentrum für Luft- und Raumfahrt) and SAFIRE (Service des Avions Français Instrumentés pour la Recherche en Environnement) who organized the experiment management and aircraft operations. We are grateful to A. Dörnbrack (DLR) for providing meteorological analysis from the ECMWF model. We acknowledge A. Schwarzenboeck and J-F Fournol (LaMP), B. Weinzierl and H. Rüba (DLR) for their active participation to the CIRCLE-2 experiment, and K. James, who reviewed the manuscript.

The publication of this article is financed by CNRS-INSU.

References

Auriol, F., Gayet, J.-F., Febvre, G., Jourdan, O., Labonnote, L., and Brogniez, G.: In situ observations of cirrus cloud scattering phase function with 22° and 46° halos: Cloud field study on 19 February 1998, J. Atmos. Sci., 58, 3376–3390, 2001.

ACPD
10, 24763–24780, 2010

Baran, A. J.: On the scattering and absorption properties of cirrus cloud, J. Quant. Spect. Rad. Tran., 89, 17–36, 2004.
Baran, A. J. and Labonnote, L.-C.: A self-consistent scattering model for cirrus. I: The solar region, Q. J. R. Meteorol. Soc., 133, 1899–1912, 2007.
Barkey, B., Bailey, M., Liou, K.-N., and Hallett, J.: Light-scattering properties of plate and column ice crystals generated in a laboratory cold chamber, Appl. Optics, 41, 5792–5796, 2002.
Bögel, W. and Baumann, R.: Test and calibration of the DLR Falcon wind measuring system by maneuvers, J. Atmos. Oceanic Technol., 8, 5–18, 1991.
Bréon, F. M. and Dubrulle, B.: Horizontally oriented plates in clouds, J. Atmos. Sci., 61, 2889–2898, 2004.
Crépel, O., Gayet, J.-F., Fournol, J.-F., and Oshchepkov, S.: A new airborne Polar Nephelometer for the measurement of optical and microphysical cloud properties. Part II: Preliminary tests, Ann. Geophys., 15, 460–470, doi:10.1007/s00585-997-0460-0, 1997.
Gayet, J.-F., Auriol, F., Oshchepkov, S., Schröder, F., Duroure, C., Febvre, G., Fournol, J.-F., Crépel, O., Personne, P., and Daugero, D.: In situ measurements of the scattering phase function of stratocumulus, contrails and cirrus, Geophys. Res. Lett., 25, 971–974, 1998.
Gayet, J.-F., Ovarlez, J., Shcherbakov, V., Ström, J., Schumann, U., Minikin, A., Auriol, F., Petzold, A., and Monier, M.: Cirrus cloud microphysical and optical properties at southern and northern midlatitudes during the INCA experiment, J. Geophys. Res., 109, D20206, doi:10.1029/2004JD004803, 2004.
Gayet, J.-F., Mioche, G., Dörnbrack, A., Ehrlich, A., Lampert, A., and Wendisch, M.: Microphysical and optical properties of Arctic mixed-phase clouds. The 9 April 2007 case study, Atmos. Chem. Phys., 9, 6581–6595, doi:10.5194/acp-9-6581-2009, 2009.
Heymsfield, A. J.: Ice particles observed in a cirriform cloud at −83°C and implications for polar stratospheric clouds, J. Atmos. Sci., 4, 851–855, 1986.
Heymsfield, A. J.: On measurements of small ice particles in clouds, Geophys. Res. Lett., 34, L23812, doi:10.1029/2007GL030951, 2007.
King, W. D.: Air flow and particle trajectories around aircraft fuselages. IV: Orientation of ice crystals. J. Atmos. Ocean. Tech., 3, 433–439, 1986.
Korolev, A. V., G. Isaac, and J. Hallett: Ice particle habits in Arctic clouds, Geophys. Res. Lett., 26, 1299–1302, 2000.
Lawson, P., Baker, B., Zmarzly, P., O'Connor, D., Mo, Q., Gayet, J.-F., and Shcherbakov, V.:

ACPD
10, 24763–24780, 2010

Microphysical and optical properties of ice crystals at South Pole Station, J. Applied Meteor Climatol., 45(11), 1505–1524, doi:10.1175/JAM2421.1, 2006.
Lefèvre, R.: Physique de la mesure de la sonde CPI pour la mesure des propriétés des cristaux de glace. Application aux observations réalisées durant la campagne ASTAR 2004, Université Blaise Pascal, Aubière, France, 186 pp., 2007.
Mariotte, E.: Oeuvres de Mr. Mariotte. Traité des couleurs, edited by: Vander, P., 1, 272–281, 1717.
Mishchenko, M. I., and Macke, A.: How big should hexagonal ice crystals be to produce halos? Appl. Opt., 38, 1626–1629, 1999.
Mioche, G., Josset, D., Gayet, J.-F., Pelon, J., Garnier, A., Minikin, A., and Schwarzenboeck, A.: Validation of the CALIPSO/CALIOP extinction coefficients from in situ observations in mid-latitude cirrus clouds during CIRCLE-2 experiment, J. Geophys. Res., 115, D00H25, doi:10.1029/2009JD012376, 2010.
Protat, A., Pelon, J., Testud, J., Grand, N., Delville, P., Laborie, P., Vinson, J.-P., Bouniol, D., Bruneau, D., Chepfer, H., Delanoe, J., Haeffelin, M., Noel, V., and Tinel, C.: Le projet RALI: Combinaison d'un radar nuage et d'un lidar pour l'étude des nuages faiblement précipitants, La Météorologie, 47, 23–33, 2004.
Pruppacher, H. R. and Klett, J. D.: Microphysics of Clouds and Precipitation, Kluwer Academic, 954 pp., 1997.
Sassen, K. and Liou, K. N.: Scattering of polarized laser light by water droplets, mixed phase and ice clouds, Part I: Angular scattering patterns, J. Atmos. Sci., 36, 838–851, 1979.
Shcherbakov, V., Gayet, J.-F., Baker, B., and Lawson, P.: Light scattering by single natural ice crystals, J. Atmos Sci., 63(5), 1513–1525, doi:10.1175/JAS3690.1., 2006a.
Shcherbakov, V., Gayet, J.-F., Jourdan, O., Ström, J., and Minikin, A.: Light scattering by single ice crystals of cirrus clouds, Geophys. Res. Lett., 33(15), L15809, doi 10.1029/2006GL026055, 2006b.
Shcherbakov, V., Gayet, J.-F., Febvre, G., Heymsfield, A. J., and Mioche, G.: Probabilistic model of shattering effect on in-cloud measurements, Atmos. Chem. Phys. Discuss., 10, 11009–11045, doi:10.5194/acpd-10-11009-2010, 2010.
Stephens, G. L., Tsay, S. C., Stackhouse, P. W., and Flatau, P. J.: The relevance of the microphysical and radiative properties of cirrus clouds to climate and climate feedback. J. Atmos. Sci., 47, 1742–1753, 1990.

ACPD
10, 24763–24780, 2010

Yang, P., Gao, B. C., Baum, B. A., Wiscombe, W. J., Hu, Y. X., Nasiri, S. L., Soulen, P. F., Heymsfield, A. J., McFarquhar, G. M., and Miloshevisch, L. M.: Sensitivity of cirrus bidirectional reflectance to vertical inhomogeneity of ice crystal habits and size distributions for Moderate-Resolution Imaging Spectroradiometer (MODIS) bands, J. Geophys. Res., 106, 17,267–17,291, 2001.

ACPD
10, 24763–24780, 2010

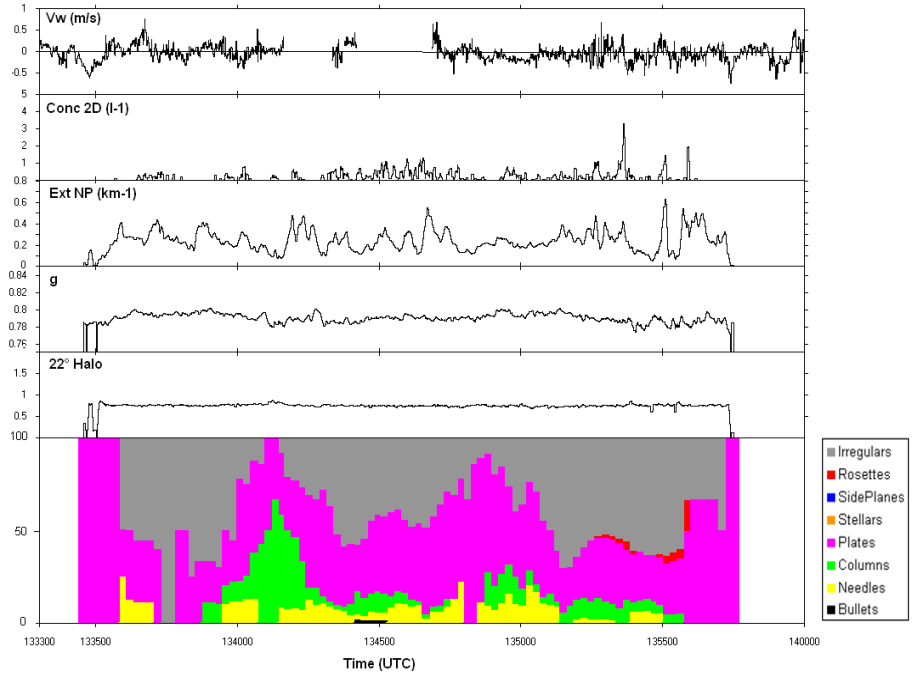

Fig. 1. Time-series of in situ parameters obtained on 16 May in cirrus cloud at 12 000 m/−59 °C and 11 600 m/−55 °C levels. Vw: vertical component of the airspeed, Conc2D: concentration of ice particles with d >100 µm (from 2D-C data), ExtNP: extinction coefficient, g: asymmetry parameter, 22° Halo ratio (see text) and CPI particle shape classification for ice crystals larger than 20 µm (averaged over 5 s. and expressed in percentages for each categories, see legends on the right side of the series).

ACPD
10, 24763–24780, 2010

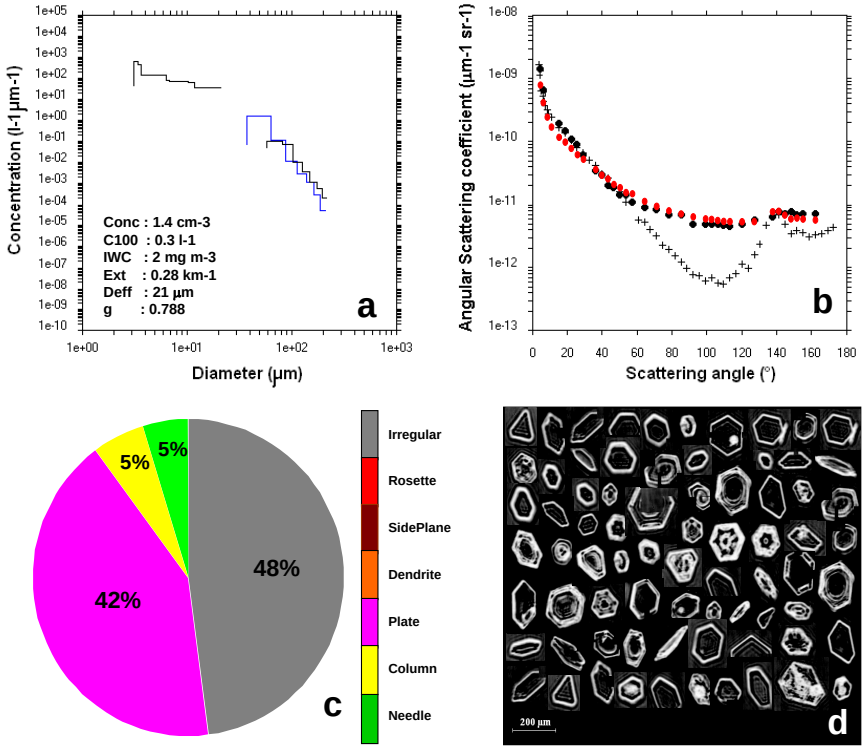

Fig. 2. Mean cirrus cloud properties averaged between 13:32:15 and 13:47:20 (see Fig. 1). **(a)**: FSSP-300, 2D-C and CPI particle size distributions with averaged values of microphysical and optical parameters; **(b)**: Scattering phase function measured by the Polar Nephelometer (filled black circle symbols) and theoretical phase function (cross symbols) calculated from the FSSP-300 size distribution assuming (spherical) ice crystals. The modeled scattering phase function is represented by filled red circle symbols. **(c)**: Pie-chart representation of the averaged particle shape classification (in terms of surface particle); **(d)**: Illustrative examples of ice particle images from the CPI instrument.

ACPD
10, 24763–24780, 2010

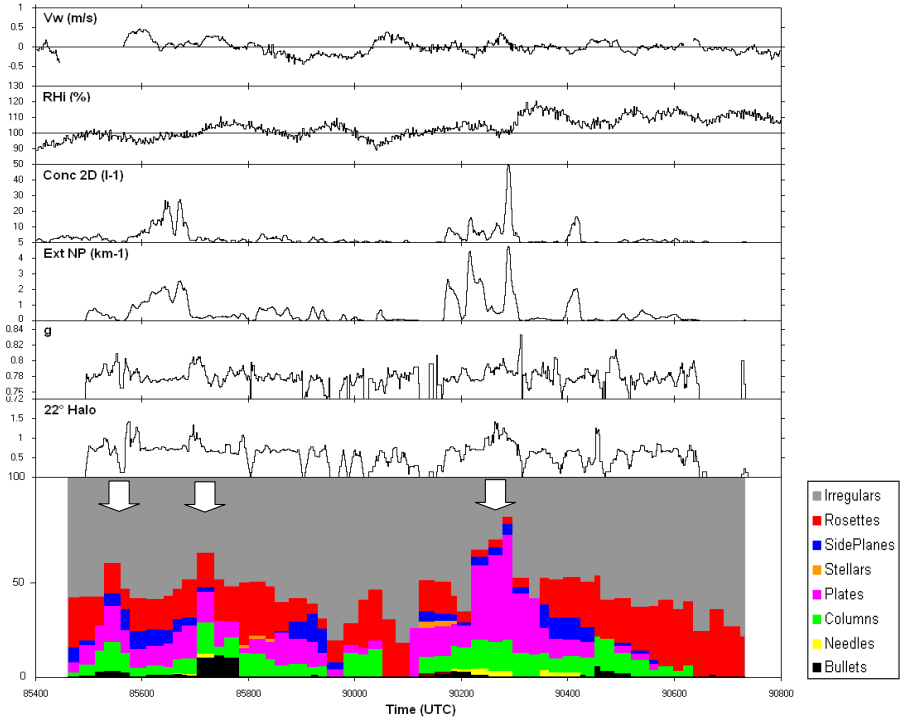

Fig. 3. Same as in Fig. 1. Time-series of in situ parameters obtained on 16 May in cirrus cloud at 7200 m/−28 °C. The relative humidity (over ice) is also indicated.

ACPD
10, 24763–24780, 2010

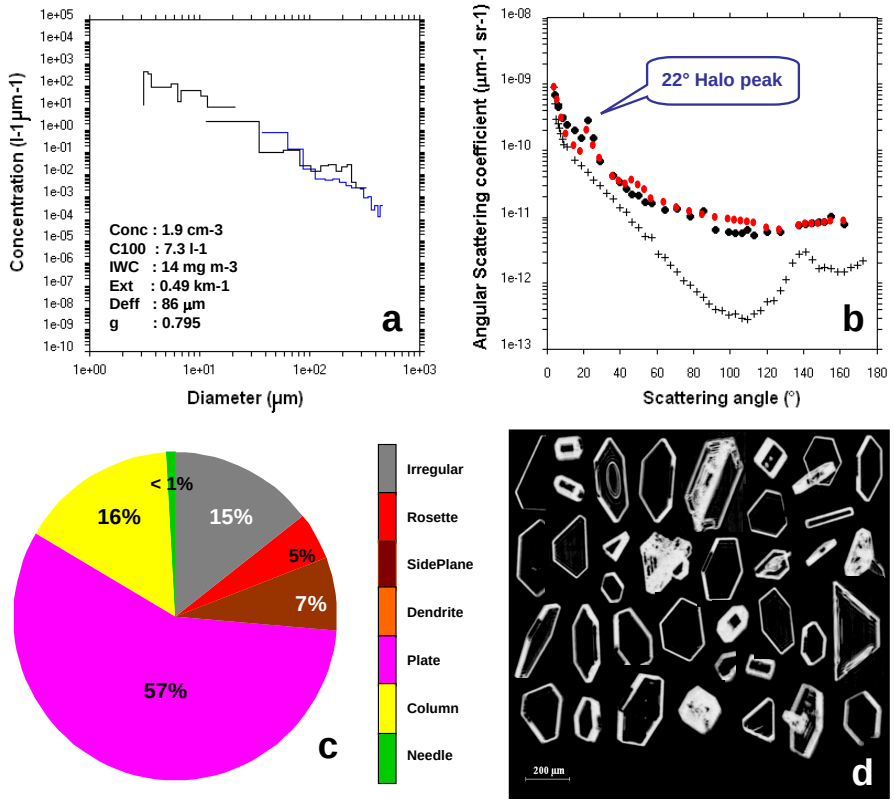

Fig. 4. Same as in Fig. 2. Mean cirrus cloud properties averaged between 09:02:10 and 09:02:30 (see Fig. 3).

ACPD
10, 24763–24780, 2010

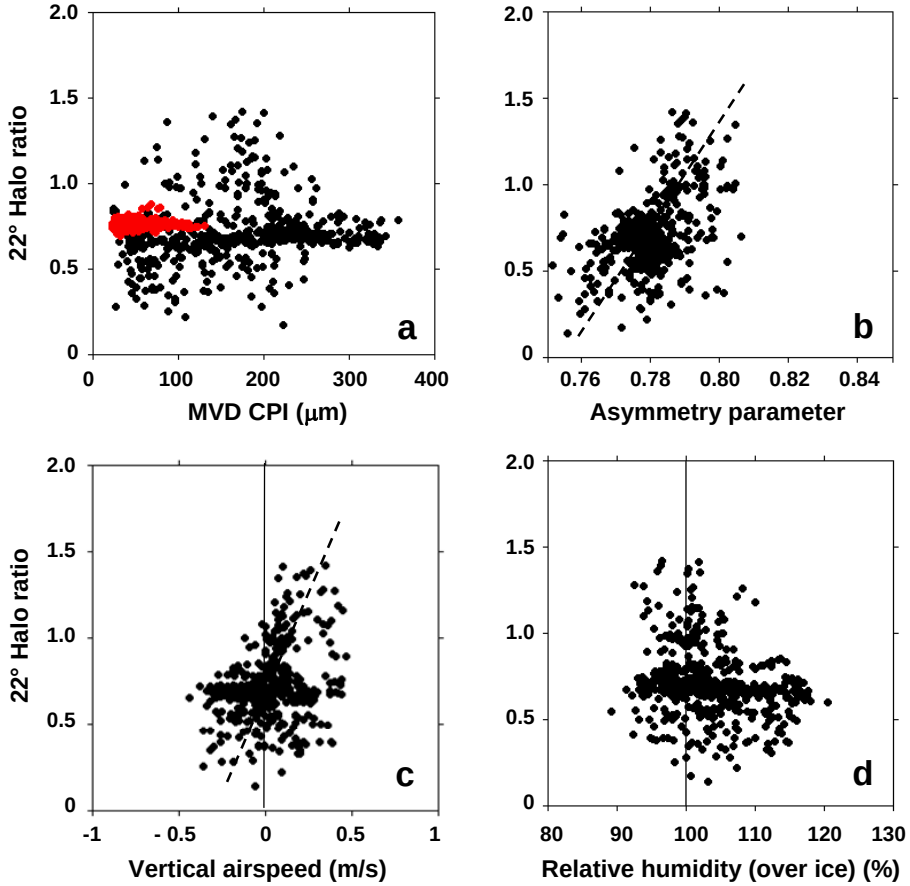

Fig. 5. Scatter plots of the halo ratio versus: **(a)** the mean volume diameter from CPI (DVM), **(b)** the asymmetry parameter, **(c)** the relative humidity over ice and **(d)** the vertical airspeed. The data relate cirrus with 22° Halo occurrence (case B, see Fig. 3). The red points on Fig. 5a concern the cirrus with no 22° Halo occurrence (case A, see Fig. 1).

ACPD
10, 24763–24780, 2010